A Journal of the Gesellschaft Deutscher Chemiker

Angewandte International Edition Chemie

GDCh

www.angewandte.org

## Accepted Article

**Title:** Activatable Small-Molecule Photoacoustic Probes that Cross the Blood-Brain Barrier for Visualization of Copper(II) in Mice with Alzheimer's Disease

**Authors:** Xuanjun Zhang, Shichao Wang, Zonghai Sheng, Zhenguo Yang, Dehong Hu, Xiaojing Long, Gang Feng, Yubin Liu, Zhen Yuan, Jingjing Zhang, and Hairong Zheng



**To be cited as:** *Angew. Chem. Int. Ed.* 10.1002/anie.201904047
*Angew. Chem.* 10.1002/ange.201904047

**Link to VoR:** http://dx.doi.org/10.1002/anie.201904047
http://dx.doi.org/10.1002/ange.201904047

WILEY-VCH

10.1002/anie.201904047

WILEY-VCH

COMMUNICATION

# Activatable Small-Molecule Photoacoustic Probes that Cross the Blood-Brain Barrier for Visualization of Copper(II) in Mice with Alzheimer's Disease

Shichao Wang, Zonghai Sheng,* Zhenguo Yang, Dehong Hu, Xiaojing Long, Gang Feng, Yubin Liu, Zhen Yuan, Jingjing Zhang, Hairong Zheng, Xuanjun Zhang*

**Abstract:** Copper enrichment in the brain is highly related to Alzheimer's disease (AD) pathogenesis, but *in vivo* tracing of $Cu^{2+}$ in the brain by imaging techniques is still a great challenge. In this work, we developed a series of activatable photoacoustic (PA) probes with low molecular weights (< 438 Da), **RPS1–RPS4**, which can specifically chelate with $Cu^{2+}$ to form radicals with turn-on PA signals in the near-infrared (NIR) region. Introducing the electron-donating group *N,N*-dimethylaniline into the probe was found to significantly enhance the radical stability and PA intensity. The best probe in the series, **RPS1**, showed a fast response (within seconds) to $Cu^{2+}$ with high selectivity and a low PA detection limit of 90.9 nM. Owing to the low molecular weight and amphiphilic structure, **RPS1** could effectively cross the blood-brain barrier (BBB) and thus allowed us, for the first time, to visualize $Cu^{2+}$ *in vivo* via PA imaging in the brains of AD mice.

Copper is the third-most abundant trace metal in the human body and plays a vital role in physiological and pathological activity. Abnormal alterations in cellular copper homeostasis are connected to serious diseases, including cardiovascular disorders, Wilson disease, and Alzheimer's disease (AD).[1] Some studies have noted that $Cu^{2+}$ enrichment in the brain has a close relationship with AD pathogenesis.[2] The redox-active $Cu^{2+}$ in the brain was implicated in the generation of reactive oxygen species (ROS), leading to the high oxidative stress that is a proposed factor in accelerating the assembly and neurotoxicity of AD amyloid-β (Aβ) fibrils.[3] Therefore, highly sensitive imaging/detection of $Cu^{2+}$ in brain of the AD is esstenial to comprehensively understand its pathological events in the brain. Currently, many fluorescent probes have been explored and

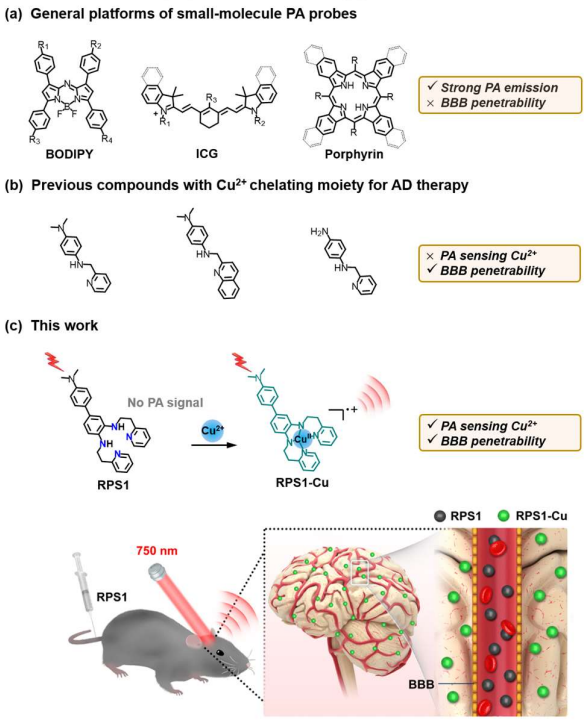


**Scheme 1**. Rational design of activatable PA probes for $Cu^{2+}$ detection in AD mouse brain. (a) Generally designed platform of small-molecule PA probes. (b) Previous compounds with $Cu^{2+}$ chelating moiety for AD therapy. (c) The target PA probe **RPS1** and schematic diagram of **RPS1** crossing the BBB and detecting $Cu^{2+}$, as observed by PA imaging.

Dr. S. Wang, G. Feng, Dr. Y. Liu, Prof. Z. Yuan, Prof. X. Zhang
Cancer Centre and Centre of Reproduction, Development and Aging, Faculty of Health Sciences, University of Macau, Macau SAR, P.R. China
E-mail: xuanjunzhang@um.edu.mo (X. Zhang)
Prof. Z. Sheng, Dr. D. Hu, X. Long, Prof. H. Zheng
Paul C. Lauterbur Research Center for Biomedical Imaging
Institute of Biomedical and Health Engineering, Shenzhen Institute of Advanced Technology, Chinese Academy of Sciences, Shenzhen 518055, P.R. China
E-mail: zh.sheng@siat.ac.cn (Z. Sheng)
Z. Yang, Prof. J. Zhang
Affiliated Hospital of Guangdong Medical University, Zhanjiang 524001, P.R. China

Supporting information for this article is given via a link at the end of the document.

applied to stain for $Cu^{2+}$ in cells and living organisms with good performance.[4] However, *in vivo* fluorescence imaging of $Cu^{2+}$ in the brain is still a great challenge due to the limited penetration depth (~ 1 mm), the obstacle for probes to cross the blood-brain barrier (BBB) and the fluorescence quenching resulting from the paramagnetic effect of $Cu^{2+}$.[5]

Compared with fluorescence technology, photoacoustic (PA) imaging combines optical imaging and ultrasound imaging into a hybrid modality, exhibiting multiscale spatial resolution with deep tissue penetration (centimeter depths).[6] Because of these advantages, PA imaging with functional probes has been widely applied in biomedical imaging, [7] disease detection,[8] and biosensing.[9] However, only a limited number of small-molecule PA probes with activatable features for detecting metal ions have been reported.[9c, 9d, 10] Moreover, to the best of our knowledge,

10.1002/anie.201904047




there has been no report of PA tracing for $Cu^{2+}$ in the brain of the animal models until now.

Theoretically, the design of small-molecule PA probes is mainly based on extending a large π-conjugated backbone, such as boron-dipyrromethene (BODIPY), indocyanine green (ICG) and porphyrin derivatives (Scheme 1a).[11] Even with strong PA emission, these probes generally have a large molecular mass that exceeds the threshold of 600 Da to cross the BBB.[12] Some of the compounds with $Cu^{2+}$ chelating moiety for AD therapy are able to cross BBB, but their insensitive absorption variation impede them as effective $Cu^{2+}$ PA probes (Scheme 1b). As unexplored PA contrast agents, aniline derivatives could form anilinyl radical complexes exhibiting near-infrared (NIR) absorption triggered by $Cu^{2+}$.[13] However, these complexes usually have a short lifetime in aqueous media because free radicals are able to abstract hydrogen from water.[14] In this work, inspired by the structures of AD drugs and aniline radicals, we designed a series of activatable PA probes, **RPS1-RPS4**, with a small molecular weight (< 438 Da) and sepcific NIR PA detection totwards $Cu^{2+}$. To tune the PA intensity and water stability of the probes, we modified the molecular structure with electron-donating and electron-accepting groups. We found that the introduction of electron-donating groups, such as *N,N*-dimethylaniline (**RPS1**), led to an amplified PA emission in the NIR region and significantly improved the stability of the probes upon detecting $Cu^{2+}$ in aqueous media. **RPS1** could effectively cross the BBB and thus allowed us for the first time to visualize $Cu^{2+}$ *in vivo via* PA imaging in AD mouse brains (Scheme 1c).

In PBS, all probe solutions exhibited a transparent color with a absorption in the ultraviolet region. After the addition of $Cu^{2+}$, the color of the solution quickly changed to green within seconds (Supporting Video 1). Structurally, **RPS1**, with the electron-donating group *N,N*-dimethylaniline, exhibited the longest absorption wavelength (713 nm) and the strongest absorbance ($\varepsilon$ > 10000) among the four probes in the presence of 1 equiv. $Cu^{2+}$ (Figure 1b, Table S1). In contrast, the relatively weaker absorbance ($\varepsilon$ < 4100) and blueshifted absorption peaks at approximately 690 nm for **RPS2-RPS4** metal chelate complexes were attributed to the smaller conjugation systems and electron acceptor groups (Figure S1b). Likewise, upon addition of $Cu^{2+}$, **RPS1** had the strongest PA emission, which was at least approximately 2.5 times greater than that of the other probes at 700 nm excitation (Figure S1c). In contrast to their lack of a PA background signal, all probes displayed a substantial PA emission upon detecting $Cu^{2+}$ except **RPS4** because of the unstable free radical formed by the **RPS4-Cu** complex. To verify the formation of a π-radical monoanion in the chelated complexes that gave rise to the NIR absorption,[13a] we conducted the MS spectra and electron paramagnetic resonance (EPR) spectroscopy of the free **RPS** probes and their chelated complexes **(RPS-Cu)** in solutions (Figure 1a, inserted Figure 1b, Figure S2, S3). The results showed that all **RPS-Cu** complexes exhibited corresponding masses and high-intensity EPR signals, which indicated the existence of an unpaired electron and the formation of radicals.

For further imaging application, the stability of these radicals in aqueous media should be evaluated because the single electron has a strong proton binding capacity and may abstract hydrogen from water molecules to quench the radical.[14] As shown in Figure S4a, **RPS4-Cu** with a naphthalene structure exhibited a fast quenching of the NIR absorption within 5 minutes. The double fluorine substituents with intensively electron-accepting ability had a damping effect on the lifetime of **RPS3-Cu** about 1 hour. The absorbance of **RPS2-Cu** in water decreased substantially within 1 hour and then remained stable over the next a few hours. Surprisingly, the introduction of *N,N*-dimethylaniline greatly increased the stability of **RPS1-Cu** to 30 hours, perhaps because the electron-donating group could stabilize the inert action of free radicals (Scheme 2, Table S1).

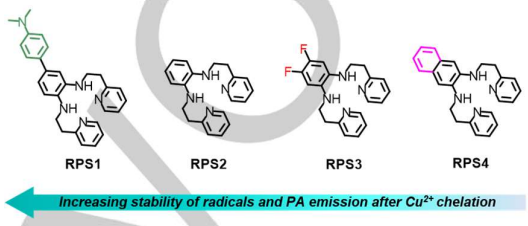


**Scheme 2**. The structures of probes **RPS1— RPS4**.

We tested the response of all probes to a variety of biologically relevant metal ions in PBS (pH 7.4, 0.02 M) and found that all **RPS1-RPS4** showed specific selectivity to $Cu^{2+}$, resulting in a unique NIR absorption (Figure S5-S8). The competition experiment in the presence of mixed metal ions ($Fe^{2+}$, $Fe^{3+}$, $Ni^{2+}$, $Co^{2+}$, $Cu^{2+}$) also showed that **RPS1** with an electron-donating group had the most superior selectivity to $Cu^{2+}$ (Figure S9). A titration experiment was conducted on **RPS1** and **RPS2** by absorption spectra in PBS and fetal bovine serum (FBS), and the results demonstrated that probes both had a good linear fit with $Cu^{2+}$ concentration. **RPS1** possessed a super low absorption limit of detection (7.2 nM) under **RPS2** (30.0 nM) and good stability in excess $Cu^{2+}$ in PBS buffer (Figures 1c, S10, S11).

Encouraged by the optimal features of **RPS1**, this probe was chosen as a potential activatable probe for subsequent PA imaging. To determine the optimal wavelength for PA imaging, the PA spectra of **RPS1** and its chelated complex were measured at wavelengths ranging from 680 to 970 nm by a Vevo LAZR imaging system.[15] As seen in Figure 1d, we found that **RPS1** had no PA signal in this broad region. Upon chelation with $Cu^{2+}$, the **RPS1** complex possessed the strongest PA signal at approximately 710 nm, followed by dampening of the PA signal. PA selection contrast to $Cu^{2+}$ of **RPS1** was overwhelmingly greater than that of other metal ions (Figure 1e). In PA quantitative analysis, the PA limit of detection was calculated to be as low as 90.9 nM. (Figure 1f). This limit of detection was lower than biological $Cu^{2+}$ level and indicated that **RPS1** had great potential for detecting $Cu^{2+}$ in the brain by PA imaging.[4b]

The temperature stability of **RPS1-Cu** was monitored by absorption in PBS. As shown in Figure S12, **RPS1-Cu** had no obvious absorption change in the range of 30 to 46 °C . Light irradiation of **RPS1** and **RPS1-Cu** within 3 hours indicated that both had good stability under intensely ambient light (Figure S13). **RPS1** also held the admired selectivity toward $Cu^{2+}$ in the presence of ROS/reactive nitrogen species (RNS) and principally reductive biomolecules (ascorbic acid, methylglyoxal, glutathione and cysteine) (Figure S14). At different pH ranges from 6.0 to 8.5, **RPS1-Cu** complex also showed a desired stability (Figure S15).

10.1002/anie.201904047

WILEY-VCH



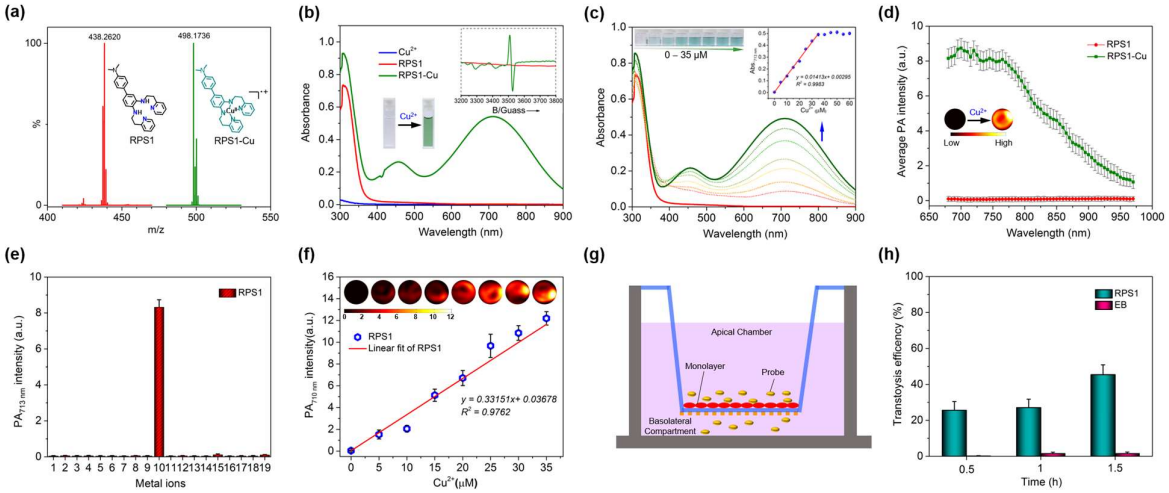


**Figure 1**. (a) Mass spectra of **RPS1** and **RPS1-Cu**. (b) The absorption spectra of **RPS1**, $Cu^{2+}$ and **RPS1-Cu** complex (all are 50 μM). The inset shows the EPR spectra of **RPS1** (2.5 mM) and **RPS1-Cu** in acetonitrile and PBS (v:v = 1:1) at room temperature. The color change of **RPS1** form transparent to deep green after treating with 1 equiv. $Cu^{2+}$. (c) Changes in the absorption spectra of **RPS1** (50 μM) after reaction with different concentrations of $Cu^{2+}$ for 10 minutes. The inset shows the color of **RPS1** solution and calibration curve of the absorbance at 713 nm for detection of $Cu^{2+}$ in the range of 0 – 35 μM. (d) PA spectra of 50 μM **RPS1** and **RPS1-Cu** from 680 to 970 nm. The inset shows the PA image of an **RPS1** and **RPS1-Cu** solution upon excitation at 710 nm. (e) PA selectivity tests for **RPS1** (50 μM, 1) upon addition of metal ions (2: $Li^+$, 3: $Na^+$, 4: $K^+$, 5: $Ca^{2+}$, 6: $Mg^{2+}$, 7: $Al^{3+}$, 8: $Fe^{2+}$, 9: $Fe^{3+}$, 10: $Cu^{2+}$, 11: $Zn^{2+}$, 12: $Ni^{2+}$, 13: $Mn^{2+}$, 14: $In^{3+}$, 15: $Co^{2+}$, 16: $Cd^{2+}$, 17: $Pb^{2+}$, 18: $Hg^{2+}$, 19: $Cu^+$; 500 μM for $Na^+$, $K^+$, and $Ca^{2+}$ and 50 μM for other metal ions) for 10 minutes. (f) Calibration curve of the PA intensity at 710 nm for detection for $Cu^{2+}$ in the range of 0 – 35 μM. Above tests were performed in 0.02 M PBS solution at pH 7.4 unless otherwise specified. (g) Schematic overview of the construction of an *in vitro* BBB model. (h) The relative transcytosis amount of **RPS1** and **EB** *in vitro* within 1.5 hours. Experiments were repeated three times, and the data are presented as the mean ± standard deviation (c, d, e, f, h).

In summary, these tests indicated that free radical of **RPS1-Cu** complex remained relatively inert toward possible *in vivo* surrounding factors. The binding affinity of **RPS1** was evaluated as $1.18 \times 10^4$ $M^{-1}$ using Benesi-Hildebrand method (Figure S16), which was in the range of affinity of the second Cu(II) binding site of A*β*.[16] To confirm **RPS1** was able to detect $Cu^{2+}$ in Aβ fibrillar aggregates, we applied the **RPS1** to Cu-Aβ aggregates and found that it has a good linear detetction towards $Cu^{2+}$ in Aβ aggregates (Figure S17).

Prior to *in vivo* PA imaging, the cytotoxicity of **RPS1** was examined in brain vascular endothelial (bEnd.3) cells by viability assay (Figure S18). The results showed that **RPS1** had negligible cytotoxicity toward bEnd.3 cells after incubation for 24 hours (probe concentration, 0-200 μM). The hemolytic analysis exhibited a low hemolysis percentage (0.5%) of red blood cells even at 40 μM **RPS1** (Figure S19). The mouse blood panel parameters showed that the values of the three groups of mice presented slight or mild variations, which indicated that **RPS1** had the advantage of low *in vivo* cytotoxicity and adequate hemocompatibility (Figure S20). Furthermore, hematoxylin and eosin (H&E) staining images of the major organs demonstrated that the probe-treated group had no distinct tissue damage compared to the control group (Figure S21). The physiological stability of the probes in nude mice was evaluated by injecting a freshly prepared **RPS1-Cu** solution (50 μM × 100 μL) into the leg muscle. Following laser irradiation (750 nm), the PA signal of the injection site was detected (Figure S22). PA imaging showed that the strong PA intensity of **RPS1-Cu** at the injection sites was much higher than that of the surrounding tissue, even after 200 minutes, indicating high in vivo stability.

To assess whether **RPS1** crosses the BBB, we measured the *in vitro* BBB-permeability efficacy of **RPS1** by transwell filters seeded with bEnd.3 cellular monolayer according to a previously reported method [17] The transwell model was separated into three typical spaces, i.e., the apical chamber, cellular monolayer, and basolateral compartment (Figure 1g). The integrity of the cellular monolayer was monitored by trans-endothelial electrical resistance (TEER) and cell staining of crystal violet. As shown in Figure S23, TEER reached a peak at about 7 days and the bEnd.3 seeded on the surface of filter integrally. For the negative control group, Evans blue (**EB**), which has been widely used as a negative tracer to assess permeability of endothelial-type barriers in normal brains without damage, was applied.[18] We chose **EB** as a negative control to ensure that the transwell model was reliable. After the addition of **EB** (10 μM) and **RPS1** (150 μM, very low toxicity to cells) into the apical chamber with integrally cellular monolayer, the absorbance of the solution on the basolateral side at 610 nm and 310 nm was measured three times every half hour, respectively. By calculating the absorbance based on Figure S24, we found that **EB** was almost completely unable to cross the cell monolayer in the transwell model. In contrast, **RPS1** had good transport capability across the cell monolayer and reached an appreciable permeability efficiency of more than 40% after 1.5 hours (Figure 1h).

Based on the above favorable results of the photophysical and PA analysis, **RPS1** was applied to PA imaging to further confirm the feasibility of detecting $Cu^{2+}$ in mouse brains. AD mice and age-matched normal mice were employed for comparison according the previous reports.[19] In one group, AD and normal mice were all injected with **RPS1** (0.5 $mg \cdot kg^{-1}$) through tail-vein intravenous treatment. In another group, AD mice were injected with PBS for the control. As shown in Figure 2a, with the aid of ultrasound imaging, a whole map of the brains with distinct borders was obtained. For the brains of normal mice treated with

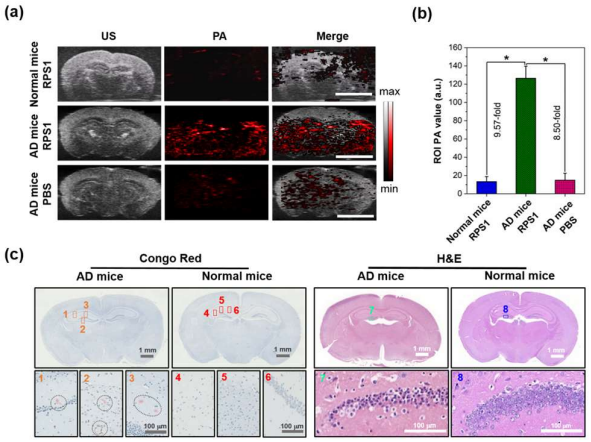


**Figure 2**. (a) Representative PA images of from the brain of normal and AD mice after 1.5 h of intravenous injection of **RPS1** and PBS. The scale bar represents 5 mm. The scan wavelength of the laser was 750 nm at 10 mJ·cm$^{-2}$. (b) The PA intensity of normal and AD mice from ROI areas. Data presented as mean ± SD, *$p$ < 0.05. (c) Histological staining of the brain slices in hippocampus region from mouse brains using Congo red and H&E.

**RPS1**, there was a weak PA signal, possibly due to the low amount of $Cu^{2+}$ detection and endogenous hemoglobin in the brain blood vessels. The brains of AD mice showed widely distributed strong PA signals throughout the whole cortex region. The AD mouse brains treated with PBS showed a weak PA signal mainly distributed over the narrow central area. The PA signal of PBS-treated AD mice has an approximate intensity but different distribution in the brain compared with probe-treated normal mice, which was possibly from the hemoglobin. The mean PA intensity in the region of interest (ROI) of AD mice treated with probe was 9.57-fold and 8.50-fold stronger than that of probe-treated normal mice and PBS-treated AD mice, respectively (Figure 2b). This result was appreciable agreement with $Cu^{2+}$ concentration ratio between AD and normal mice brain that was determined by inductively coupled plasma-atomic emission spectrometry (ICP-AES) (Table S2). Higher resolution and deeper *ex vivo* PA imaging of brains were performed on advanced three-dimensional (3D) PA system. As shown in Figure S25, the cerebral blood vessels (red ellipses dash) in normal and AD mice treated with **RPS1** became more visible. Along the cerebral blood vessels, the cerebral cortex region of AD mice showed strong PA signals, whereas the same region of normal mice displayed dim photoacoustic signals. The green-red color of PA images represented a higher $Cu^{2+}$ concentration in cortex regions (blue arrows). This phenomenon was more obvious in 3D PA imaging (Supporting Video 2_3D and Video 3_3D). To determine the biodistribution of **RPS1** in living mice, *ex vivo* PA images of major organs were acquired. As shown in Figure S26, compared with control group, photoacoustic signals of the liver, kidney and brain of **RPS1**-treated group were significantly enhanced after intravenous injection of probe for 1.5 h, indicating that the probe was mainly metabolized by liver and kidney and enriched in the brain. After PA imaging, the brains were prepared with slices and stained by Congo red and H&E for observation. Notably, the Congo red staining AD brain slices showed a mass of plaques deposition in hippocampus region. The shrunken cell nucleuses were also found in this region from H&E staining AD brain slices. These are significantly neurodegenerative characters of AD compared with normal mice (Figure 2c). Thus, this result provided visual evidence that **RPS1** could effectively cross the BBB and detect $Cu^{2+}$ in the whole brains of normal and AD mice by the PA technique. In addition, the study also verified the higher level of $Cu^{2+}$ in AD mice compared than in normal mice by PA imaging for the first time.

Different from conventional PA probes with extended π-conjuation, **RPS** probes with low molecular weight that can specifically chelate $Cu^{2+}$ to form radicals with turn-on PA response in the NIR region. Introducing electron-donating group *N,N*-dimethylaniline was found to dramatically improve the stability of the probe-Cu radical and enhance the NIR PA intensity. Owing to the low molecular weight and amphiphilic structure, **RPS1** could effectively corss BBB and achieve the visualization of $Cu^{2+}$ in the whole brain of AD mice by PA imaging. This work provided a new design of PA probes and broaden the PA sensing application in the brain. We anticipate that this type of small-molecular-weight probe will find a potential application in AD diagnosis, drug screening and treatment evaluation.

## Acknowledgements

This work was supported by the National Key Research and Development Program of China: Scientific and technological innovation cooperation of Mainland and Macao (2017YFE0120000), the Macao Science and Technology Development Fund (Grant Nos. 019/2017/AMJ, and 082/2016/A2), the Natural Science Foundation of China (91859117, 81571745, 81771906). Shenzhen Double Chain Grant [2018]256 and Natural Science Foundation of Guangdong Province (2014A030312006). We thank Shenzhen Key Laboratory of Ultrasound Imaging and Therapy (ZDSYS20180206180631473). We are also grateful to Jian Su for assistance with the EPR measurements and Prof. Rongqin Zheng from the third people's hospital of Sun Yat-Sen University for 3D photoacoustic imaging.

## Conflict of interest

The authors declare no competing financial interests.

**Keywords:** photoacoustic probe • blood-brain barrier• Alzheimer's disease • cupric ion

[1] a) L. Zeng, E. W. Miller, A. Pralle, E. Y. Isacoff, C. J. Chang, *J. Am. Chem. Soc.* **2006**, *128*, 10-11; b) T. Hirayama, G. C. Van de Bittner, L. W. Gray, S. Lutsenko, C. J. Chang, *Proc. Natl. Acad. Sci. U. S. A.* **2012**, *109*, 2228-2233.

[2] K. P. Kepp, *Chem. Rev.* **2012**, *112*, 5193-5239.

[3] a) G. Multhaup, A. Schlicksupp, L. Hesse, D. Beher, T. Ruppert, C. L. Masters, K. Beyreuther, *Science* **1996**, *271*, 1406-1409; b) K. J. Barnham, C. L. Masters, A. I. Bush, *Nat. Rev. Drug Discov.* **2004**, *3*, 205-214; c) A. Rauk, *Chem. Soc. Rev.* **2009**, *38*, 2698-2715.

[4] a) J. A. Cotruvo, Jr., A. T. Aron, K. M. Ramos-Torres, C. J. Chang, *Chem. Soc. Rev.* **2015**, *44*, 4400-4414; b) E. L. Que, D. W. Domaille, C. J. Chang, *Chem. Rev*. **2008**, *108*, 1517-1549.

[5] a) G. Sivaraman, M. Iniya, T. Anand, N. G. Kotla, O. Sunnapu, S. Singaravadivel, A. Gulyani, D. Chellappa, *Coordin. Chem. Rev.* **2018**, *357*, 50-104; b) O. Veiseh, C. Sun, C. Fang, N. Bhattarai, J. Gunn, F. Kievit, K. Du, B. Pullar, D. Lee, R. G. Ellenbogen, J. Olson, M. Zhang, *Cancer Res.* **2009**, *69*, 6200-6207; c) Y. S. Zhang, J. Yao, *Trends Biotechnol.* **2018**, *36*, 403-414; d) T. Branch, P. Girvan, M. Barahona, L. Ying, *Angew. Chem. Int. Ed.* **2015**, *54*, 1227-1230.

[6] a) C. Kim, C. Favazza, L. V. Wang, *Chem. Rev.* **2010**, *110*, 2756-2782; b) L. V. Wang, J. Yao, *Nat. Methods* **2016**, *13*, 627-638.

[7] a) S. Mallidi, G. P. Luke, S. Emelianov, *Trends Biotechnol.* **2011**, *29*, 213-221; b) E. I. Galanzha, E. V. Shashkov, T. Kelly, J. W. Kim, L. Yang, V. P. Zharov, *Nat. Nanotechnol.* **2009**, *4*, 855-860; c) X. Wang, D. L. Chamberland, D. A. Jamadar, *Opt. Lett.* **2007**, *32*, 3002-3004; d) Y. Wang, X. Hu, J. Weng, J. Li, Q. Fan, Y. Zhang, D. Ye, *Angew. Chem. Int. Ed.* **2019**, *58*, 4886-4890. e) Y. Jiang, P. K. Upputuri, C. Xie, Z. Zeng, A. Sharma, X. Zhen, J. Li, J. Huang, M. Pramanik, K. Pu, *Adv. Mater.* **2019**, 31, e1808166; f) X. Zhen, J. Zhang, J. Huang, C. Xie, Q. Miao, K. Pu, *Angew. Chem. Int. Ed*. **2018**, 57, 7804-7808.

[8] a) C. J. Reinhardt, E. Y. Zhou, M. D. Jorgensen, G. Partipilo, J. Chan, *J. Am. Chem. Soc.* **2018**, *140*, 1011-1018; b) S. C. Wang, Z. Li, Y. B. Liu, G. Feng, J. Zheng, Z. Yuan, X. J. Zhang, *Sensor Actuat. B-Chem.* **2018**, *267*, 403-411; c) J. Zhang, X. Zhen, P. K. Upputuri, M. Pramanik, P. Chen, K. Pu, *Adv. Mater.* **2017**, *29*, 1604764; d) B. Shi, X. Gu, Q. Fei, C. Zhao, *Chem. Sci.* **2017**, *8*, 2150-2155; e) Q. Chen, C. Liang, X. Sun, J. Chen, Z. Yang, H. Zhao, L. Feng, Z. Liu, *Proc. Natl. Acad. Sci. U. S. A.* **2017**, *114*, 5343-5348; f) K. Pu, A. J. Shuhendler, J. V. Jokerst, J. Mei, S. S. Gambhir, Z. Bao, J. Rao, *Nat. Nanotechnol.* **2014**, *9*, 233-239; g) J. Zhang, X. Zhen, J. Zeng, K. Pu, *Anal. Chem.* **2018**, *90*, 9301-9307; h) E. Y. Zhou, H. J. Knox, C. J. Reinhardt, G. Partipilo, M. J. Nilges, J. Chan, *J. Am. Chem. Soc.* **2018**, *140*, 11686-11697.

[9] a) H. J. Knox, J. Hedhli, T. W. Kim, K. Khalili, L. W. Dobrucki, J. Chan, *Nat. Commun.* **2017**, *8*, 1794; b) H. J. Knox, T. W. Kim, Z. Zhu, J. Chan, *ACS Chem. Biol.* **2018**, *13*, 1838-1843; c) S. Roberts, M. Seeger, Y. Jiang, A. Mishra, F. Sigmund, A. Stelzl, A. Lauri, P. Symvoulidis, H. Rolbieski, M. Preller, X. L. Dean-Ben, D. Razansky, T. Orschmann, S. C. Desbordes, P. Vetschera, T. Bach, V. Ntziachristos, G. G. Westmeyer, *J. Am. Chem. Soc.* **2018**, *140*, 2718-2721; d) H. Li, P. Zhang, L. P. Smaga, R. A. Hoffman, J. Chan, *J. Am. Chem. Soc.* **2015**, *137*, 15628-15631; e) Y. Liu, S. Wang, Y. Ma, J. Lin, H. Y. Wang, Y. Gu, X. Chen, P. Huang, Adv. Mater. **2017**, *29*, 1606129.

[10] a) L. Zeng, G. Ma, H. Xu, J. Mu, F. Li, X. Gao, Z. Deng, J. Qu, P. Huang, J. Lin, *Small* **2019**, *15*, e1803866; b) N. W. Pino, J. Davis, 3rd, Z. Yu, J. Chan, *J. Am. Chem. Soc*. **2017**, 139, 18476-18479.

[11] a) H. J. Knox, J. Chan, *Acc. Chem. Res.* **2018**, *51*, 2897-2905; b) L. Zeng, G. Ma, J. Lin, P. Huang, *Small* **2018**, *14*, e1800782; c) S. Banala, S. Fokong, C. Brand, C. Andreou, B. Krautler, M. Rueping, F. Kiessling, *Chem. Sci.* **2017**, *8*, 6176-6181.

[12] a) R. C. Young, R. C. Mitchell, T. H. Brown, C. R. Ganellin, R. Griffiths, M. Jones, K. K. Rana, D. Saunders, I. R. Smith, N. E. Sore, et al., *J. Med. Chem*. **1988**, *31*, 656-671; b) K. Serdons, T. Verduyckt, D. Vanderghinste, P. Borghgraef, J. Cleynhens, F. Van Leuven, H. Kung, G. Bormans, A. Verbruggen, *Eur. J. Med. Chem*. **2009**, *44*, 1415-1426.

[13] a) G. Buncic, Z. Xiao, S. C. Drew, J. M. White, A. G. Wedd, P. S. Donnelly, *Chem. Commun.* **2012**, *48*, 2570-2572; b) M. Bhadra, J. Y. C. Lee, R. E. Cowley, S. Kim, M. A. Siegler, E. I. Solomon, K. D. Karlin, *J. Am. Chem. Soc.* **2018**, *140*, 9042-9045; c) C. C. Chang, H. Yueh, C. T. Chen, *Org. Lett.* **2011**, *13*, 2702-2705.

[14] a) I. Fenoglio, M. Tomatis, D. Lison, J. Muller, A. Fonseca, J. B. Nagy, B. Fubini, *Free Radic. Biol. Med*. **2006**, *40*, 1227-1233; b) W. K. Pogozelski, T. D. Tullius, *Chem. Rev.* **1998**, *98*, 1089-1108.

[15] Z. Sheng, B. Guo, D. Hu, S. Xu, W. Wu, W. H. Liew, K. Yao, J. Jiang, C. Liu, H. Zheng, B. Liu, *Adv. Mater.* **2018**, *30*, e1800766.

[16] M. W. Beck, J. S. Derrick, R. A. Kerr, S. B. Oh, W. J. Cho, S. J. Lee, Y. Ji, J. Han, Z. A. Tehrani, N. Suh, S. Kim, S. D. Larsen, K. S. Kim, J. Y. Lee, B. T. Ruotolo, M. H. Lim, *Nat. Commun*. **2016**, 7, 13115.

[17] D. Ni, J. Zhang, W. Bu, H. Xing, F. Han, Q. Xiao, Z. Yao, F. Chen, Q. He, J. Liu, S. Zhang, W. Fan, L. Zhou, W. Peng, J. Shi, *ACS Nano* **2014**, *8*, 1231-1242.

[18] a) M. Kaya, B. Ahishali, in Permeability Barrier, *Springer*, **2011**, pp. 369-382; b) K. H. Shim, K. H. Jeong, S. O. Bae, M. O. Kang, E. H. Maeng, C. S. Choi, Y. R. Kim, J. Hulme, E. K. Lee, M. K. Kim, S. S. An, *Int. J. Nanomedicine* **2014**, 9 Suppl 2, 225-233.

[19] Y. Yu, L. Zhang, C. Li, X. Sun, D. Tang, G. Shi, *Angew. Chem*. **2014**, 126, 13046-13049.

10.1002/anie.201904047

WILEY-VCH



**Entry for the Table of Contents**

Layout 2:

COMMUNICATION

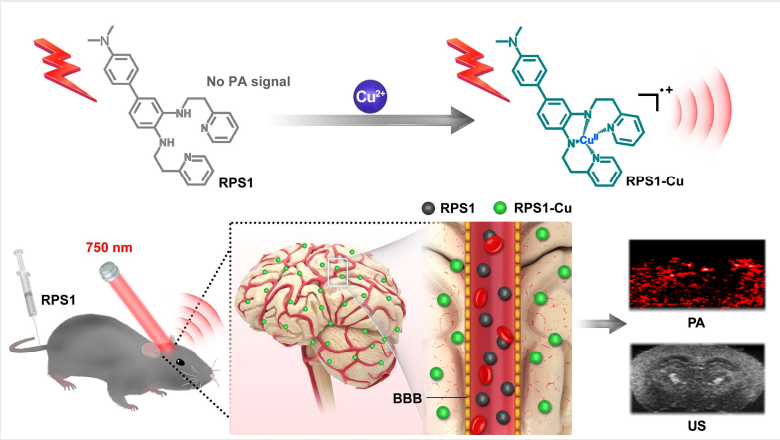


*Shichao Wang, Zonghai Sheng,* Zhenguo Yang, Dehong Hu, Xiaojing Long, Gang Feng, Yubin Liu, Zhen Yuan, Jingjing Zhang, Hairong Zheng, Xuanjun Zhang**

***Page No. – Page No.***

**Activatable Small-Molecule Photoacoustic Probes that Cross the Blood-Brain Barrier for Visualization of Copper(II) in Mice with Alzheimer's Disease**

**Photoacoustic Imaging of Copper(II) in Brain.** Small-molecule probe **RPS1** can selectively bind to $Cu^{2+}$ forming radical with turn-on photoacoustic response in the NIR region. **RPS1** can effectively cross blood-brain barrier and image copper(II) in AD mouse brain.